Switched reluctance motor design for electric vehicles based on harmonics and back EMF analysis

Abid Ali Shah Bukhari[1] ✉, Belema Prince Alalibo[1], Wenping Cao[1], Zhengyu Lin[1], Shahid Hussain Shaikh[2], Toufique Ahmed Soomro[3], Shahzeb Ansari[2], Fayyaz Ali Jandan[2]

[1]School of Engineering and Applied Sciences, Aston University, Aston Triangle, Birmingham, UK
[2]Department of Electrical & Electronic Engineering, Quaid-e-Awam University College of Engineering Science & Technology Larkana, Sindh-Pakistan
[3]School of Computing and Mathematics, Charles Sturt University, Australia
✉ E-mail: bukhars2@aston.ac.uk

Abstract: Permanent magnet synchronous motors are widely accepted in automotive applications. The high torque density, high rotational speed with maximum efficiency in electric vehicle applications is technically challenging for motor design. However, these machines are expensive and difficult to work at high-temperature harsh environment due to permanent magnets demagnetisation features. Alternatively, switched reluctance motors can provide similar output characteristics and a wider speed. Thus these are considered to be more fault tolerant and more reliable. This study proposes a 20 kW, three-phase switched reluctance motor and analyse its overall performance and harmonic contents. The study is conducted by optimising the slot filling factor, excitation voltage and switching sequence of an asymmetrical half bridge converter. A finite element model is used to predict the core and copper losses and other influencing parameters. Simulation results are presented and analysed the effectiveness of the proposed switched reluctance motor (SRM).

1 Introduction

Currently transport related air pollution is a severe matter of concern, particularly in populated urban areas, such as, Beijing, Karachi, Ankara, and Mexico. In general 25% of worldwide CO_2 emanations are due to transportation. In addition to CO_2, SO_x, and NO_x are also produced [1]. A breakdown of global CO_2 emissions from fossil fuel is shown in Fig. 1. It is predicted that the energy consumed by transport system could be doubled by 2050 [5, 6]. In the meantime, the total CO_2 emissions are expected to reduce to half. In order to meet this challenge, significant use of electrified vehicles is needed to replace conventional internal combustion-engine-based vehicles. It is essential to develop low-carbon technologies and to establish a low-carbo economy. In this method, electric vehicles have turned into the key authentic and logical research around the globe in the 21st century. The development of electric vehicle (EV) and the power transfer process is shown in Figs. 2*a* and *b*. The most widely used electric motor for traction application is the permanent magnet synchronous motors (PMSMs) [8]. This is because of the reality that permanent magnet enables these motors to achieve high torque densities which actually makes this machine very small [9, 10]. On the other hand, the inclusion of uncommon rare-earth material in permanent magnets which is very costly and whose extraction and refining are related to non-immaterial ozone depleting substance outflows [9]. In this manner,
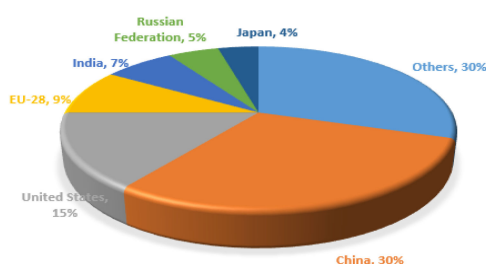

Fig. 1 *Global CO_2 emissions from fossil fuel combustion and some industrial processes [2–4]*

electric machines without rare earth materials exhibit an expanding interest to reach and accomplish comparable performance of different machines. Among the distinctive existing magnet free machines, there is much interest in switched reluctance motor for the propulsion of electric and hybrid electric vehicles due to rugged construction and simple design with the capability to operate in hazard free environment at very high speed [11–13]. The electromagnetic modelling offers the enhancement that possibly lead to more anticipated output characteristics such as flux linkage, output torque, speed, power loss and flux density can be evaluated. Since the optimised design of electrical machines are determinant factors, several methods of switched reluctance motor (SRMs) design and operation could be found in the reference. An investigation of finding faults through current harmonics has been presented in [14]. The production of current harmonics with instantaneous torque equation has been predicted in [15]. The 12/8 segmented rotor type SRM for vehicle cooling application is presented in [16]. For enhancing the performance of SRM, the autotransformer winding method for each phase has been considered in [17]. The reduction of vibration and acoustic noise technique has been presented on the use fast dc, first-, second- and third-harmonic contents in [18]. The double rotor SRM configuration has been used in [19, 20] to investigate the performance, electromagnetic forces and harmonic distortion characteristics. The harmonic superposition at low computational cost SRM has been introduced in [21]. An investigation on SRM drive fed by pulse width modulation is carried out in [22]. A dynamic model of three-phase 12/8 SRM with adopted variable angle current chopping control is proposed in [23]. The optimal number of winding turns and changing shape of the winding slot of 12/8 SRM is presented in [24]. The model of tooth concentrated winding along with magnetic saturation and its effect on MMF harmonics and iron losses have been presented in [25]. However, the main significant harmonic contents and back emf production is not available theoretically. The author's main approach is to use the principal of machine design and to analyse the harmonics and back EMF by the variation of slot filling factor, excitation voltage and switching sequence and the effects of these changing variables on the machine performance such as average torque, speed,
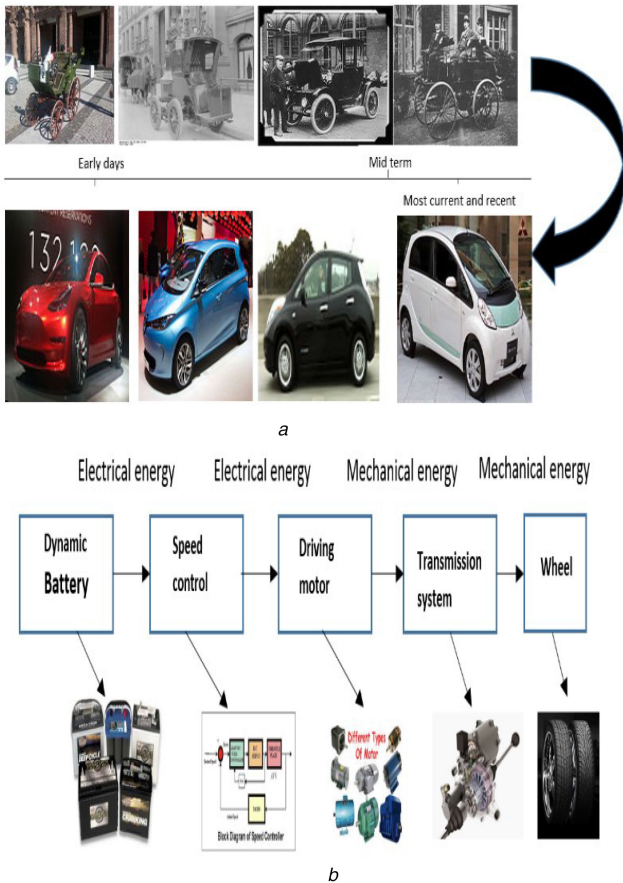
Fig. 2 *The time to time growth and stages of EV*
(a) Development of electric vehicles, *(b)* power transfer process of electric vehicle [7, 8]

instantaneous energy, core and copper losses. As these analyses can be the responsible factor for the efficiency improvement of electric motor. Initially, the 12/8 SRM is designed in the AutoCAD and is imported into infolytica magnet software and the characteristics of Torque, speed, flux linkages, current, voltage with power loss calculations are calculated by finite element method through the infolytica magnet software, then generated harmonics and back emf are analysed from the data through fast Fourier transform (FFT) analysis MATLAB software. This paper has been organised as follows: In Section 1, detail introduction and research background of the research with respect to energy scenario issues are discussed in addition to the development of electric vehicles. The SRM modelling and its associated equations have been discussed in Section 2. SRM development including design issues with various aspects of modelling with essential design characterisation and simulation results have been discussed in Section 3. The brief application and future perspective trends have been discussed in Section 4.

2 SRM modelling

To design the 12/8 SRM, the best possible parameters have been considered. Thus the strategy has been established on the present awareness which exists about the operational principals of SRMs and previous research. The equation can be developed as follows:

$$V_{dc} = R_a I_a + L\frac{di}{dt} + Eb \qquad (1)$$

The relationship between the source voltage, flux linkage (Ψ) and the rotor position angle (θ) is

$$V_{dc} = R_a I_a + L_a\frac{dia}{dt} + \frac{\partial \psi a}{\partial \theta}\frac{d\theta}{dt} \qquad (2)$$

Sincee $\psi a = L_a I_a$

Table 1 Design specifications of the 12/8 SRM

Parameter	Symbol	Value	Units
stator diameter	ds	250	mm
rotor diameter	dr	130	mm
air-gap	g	0.75	mm
machine length	l	200	mm
number of stator poles	Ns	20	—
number of rotor poles	Nr	8	—
stator pole arc	βs	12	o
rotor pole arc	βr	22	o
number of phases	m	3	—
peak speed	nN	2800	rpm
phase voltage	Vdc	200	V
number of turns	Np	7	turns
shaft diameter	dsh	40	mm
rotor yoke thickness	yr	23.6	mm
stator yoke thickness	ys	15.8	mm
rotor pole length	lr	10.9	mm
stator pole length	ls	44.7	mm
rotor pole width	tr	25.6	mm
stator pole width	ts	23.6	mm
average torque	Tav	64.9	Nm

$$V_{dc} = R_a I_a + L_a\frac{dia}{dt} + \frac{\partial La}{\partial \theta}\frac{d\theta}{dt} \qquad (3)$$

The instantaneous electromagnetic torque produces by (Ta) of the switched reluctance machine by one phase:

$$T = \frac{1}{2}i^2\frac{\partial La}{\partial \theta} \qquad (4)$$

$$T - T_L = J\frac{d\omega}{dt} + B\omega \qquad (5)$$

Whereas T represents the electromagnetic torque of the motor and T_L is the torque produced by the load, and $\omega = (d\theta/dt)$ is the speed of the motor. The above equations are used to model the SRM.

3 Results and discussions

The 12/8 switched reluctance motor has been simulated with the specifications shown in Table 1. The stack length of 200 mm have been maintained to get the sensibly proportioned machine and the basic switching pattern for high speed has been adopted which energises the phase-1 at 0, and open at 15°, when overlaps ceases. This pattern repeats after every 45°. So a periodic sequence to is ON-0-OFF-15-ON-45 has been adopted throughout the simulation. The other switches follow the same pattern in sequence with the delay by 15° at each time successively. The 12/8 SRM model with mesh view and magnetic flux density of 1.6 Tesla is shown is Figs. 3a–c. The graph of speed and generated torque is shown is Fig. 4. Firstly the identical scheme of SR motor, only one switch with single diode per phase converter topology was adopted but the results were not up to the mark as per author's satisfaction in addition to the results there were uncertain oscillating effects in the machine performance in the middle of (0–500 RPM) which is not desirable for the electric vehicle application.

Then further the author tried another configuration and asymmetric bridge converter topology has been used to drive the proposed SR motor, it has two switches per phase with two diodes which is the main advantages due independent and flexible controlling and favourable for high speed machine operation thus overlap between adjacent current is possible however compromise is made between costs due to extra switches and diode per phase. In order to control the current magnitude the current source of piecewise liner (PWL) as an input source for excitation winding has been provided which is shown in Fig. 5. The nonlinear lamination material Newcore 1000/65 selected for the core the
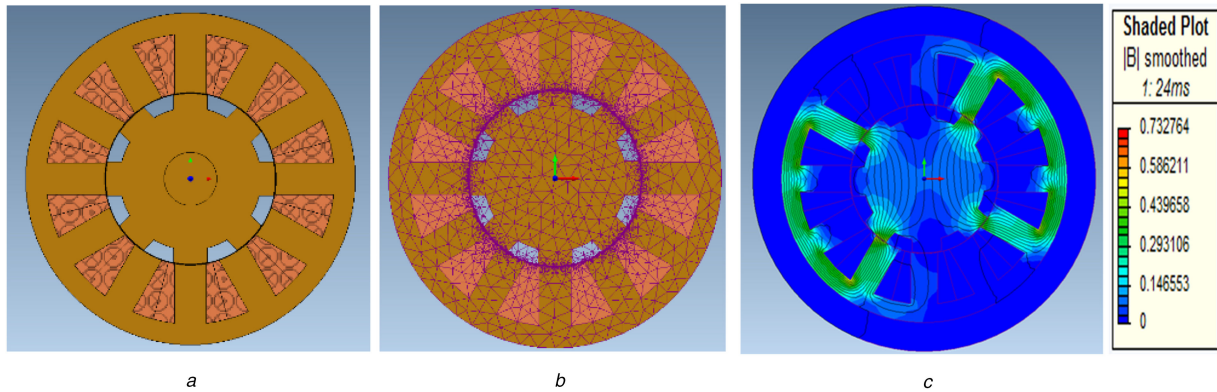
Fig. 3 *The projected design of*
(a) 12/8 SRM model, *(b)* Mesh view, *(c)* shows the flux function view with 1.6 T
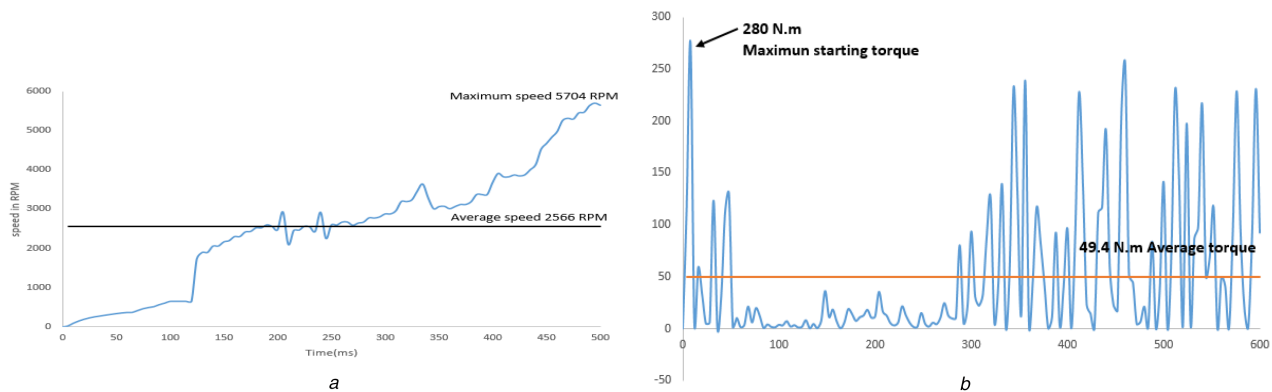

Fig. 4 *The simulation results of 12 by 8 SRM*
(a) Speed vs time graph and, *(b)* starting and average torque produced by the 12/8 SRM
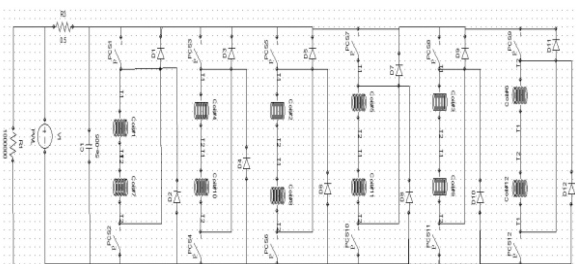

Fig. 5 *Asymmetric bridge converter topology for driving 12/8 SR motor*

graph of magnetic permeability of Newcore (1000/65) and the losses are shown in Figs. 6a and b. The transient simulation with the number of turns and cross sectional area of turn to get the sensible results of 200, 150, 100 and 50 turns with (3.84–6.2) mm^2 which is intended to represent 40, 50 and 60% slot filling factor (packing) in the slot area as shown in Tables 2 and 3, which depicts the results of energy, torque, speed, flux linkage, current, voltage and losses produced by proposed machine. In this test the number of turns are constant whereas the stranded area of the conductor has been varied. The load-driven transient simulation carried out at 500 milliseconds, it can be noted that the machine has good starting torque up to 280 N m but rapidly falls off. The reason is the inductive leg effect when switches are turned ON and OFF, and the motor provides the effective average torque from 10 to 50 N m.

The voltage of coil 1–2, 2–3, and 1–3 area taken for the data analysis of harmonics and back emf whereas, it is assumed that the same voltages are flowing in other coils 4,5 and 6. So that is why the reaming coil's voltage have not been taken into account in this research paper. The average values of voltage from coil (1–2, 2–3 and 1–3) are exported into excel file to get the back emf voltage and the same data is imported to MATLAB for harmonic FFT (FFT) analysis. The graph of harmonics and back emf at changing filling factor (40–55%) while changing stranded conductor area is shown is Fig. 7. All the data achieved from simulation results have
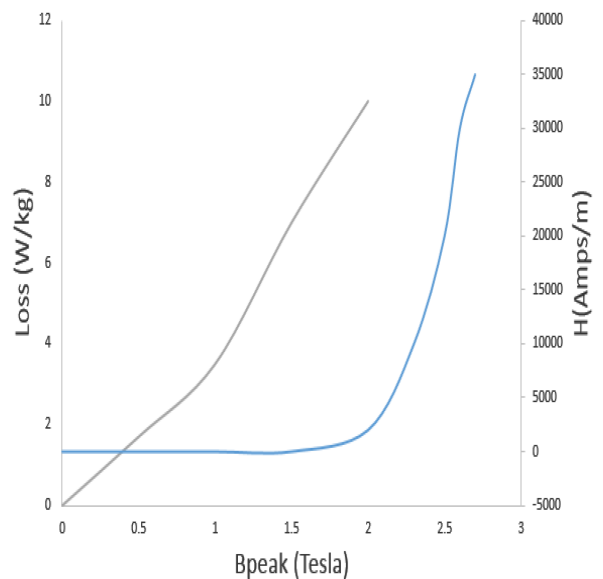

Fig. 6 *The graph of New Core 1000/65 material*
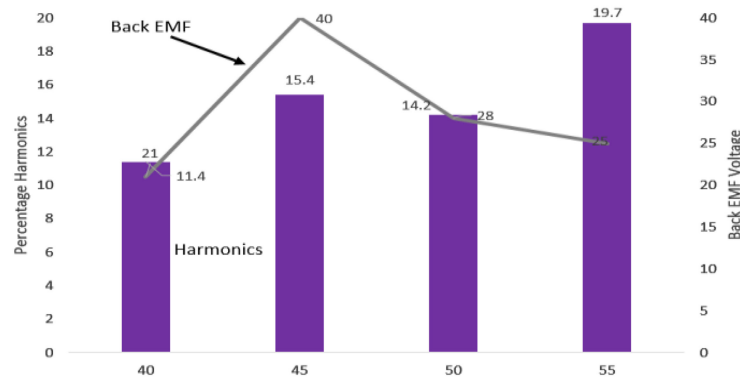*(a)* Power loss (w/kg), and *(b)* the magnetic permeability

been process through same method as mentioned above for conducting the tests. In the second test, the stranded area has been kept constant and number of turns are varied Tables 4 and 5 shows the data of energy, torque, speed, flux linkage, current and voltage and losses of the machine while changing number of turns. The harmonic and back emfs produced are shown in Fig. 8. In the third test excitation voltage are varied while keeping all the parameters of filling factor at constant values. Tables 6 and 7 shows the data achieve after simulation of energy, torque, speed, flux linkage, current, voltage while changing excitation voltage and losses. This shows that the torque and speed are affected while decreasing voltage from 200 to 50 and there is also similar effect on flux

Table 2 Energy, torque, speed, flux linkage while changing filling factor and fixing the size

| Fill factor, area | Energy | | Torque in, N m | | Speed in, degree/sec | | Flux linkage |
	Inst	Co-energy	Start	Avg	Max	Avg	Max
40%, 3.84 mm	3.8	5.5	132	10	6750	4855	0.06
45%, 3.84 mm	22	58	210	49	121,00	6456	0.17
50%, 3.84 mm	35	98	210	60	15,000	9021	0.15
55%, 3.84 mm	31	77	280	71	17,000	11,740	0.14

Table 3 Current, voltage and losses while changing the filling factor by constant turns and varied standard area

Fill factor, area	Current	Voltage	Copper losses	Iron loss
40% 3.84 mm	5.18	3.88	104	29.3
45% 3.84mm	30.5	6.5	87.7	31.9
50% 3.84 mm	32.6	27	161	39.6
55% 6.2 mm	19.2	38.3	103	48.2

Fig. 7 *Harmonics and back emf results with the slot filling factor and the stranded area*

Table 4 Energy, torque, speed and flux linkage while changing filling factor by constant standard area and varied turns

| Fill factor, turns | Energy | | Torque in, N m | | Speed in, degree/sec | | Flux linkage |
	Inst	Co-energy	Start	Avg	Max	Avg	Max
40%, 50	3.8	5.5	132	10.4	6750	4855	0.06
45%, 56	19.7	47.7	275	41.4	16,200	9739	0.135
50%, 62	12	25	270	27	11,000	5200	0.14
55%, 68	11.4	25	255	23	16,500	7993	0.11

Table 5 Current, voltage and losses while changing filling factor by constant standard area and varied turns

Fill factor, area	Current	Voltage	Ohmic loss	Iron loss
40% 3.84 mm	5.18	3.88	104	29.3
45% 3.84 mm	13	29	74.9	36.7
50% 3.84 mm	10.2	12.7	24.5	32.3
55% 3.84 mm	7.4	13	30.8	26

linkage. Fig. 9, shows the harmonics and back emf graph while varying excitation voltage. It reflect that there is a direct relation between harmonics and back emf with excitation voltage so it can be predicted that, higher the supply excitation voltage then higher will be the back emf and harmonic produced in the machine.

The fourth test is carried out at changing excitation switching sequence. As there are 12 switches, so different switching angles are provided to it. The following switching angles are provided to the coils which are described as follows:

coil1, 7 and coil 4, 10 are provide switching angle ON: 0, OFF: 15 and again ON: 45. Coil 2, 8 and coil 5, 11 are provided ON: 9, OFF: 24 and again ON: 54 coil 3, 9 and coil 6, 12 are provided ON: 18, OFF: 33 and again ON: 63. It can be seen that in each phase there is angle difference of 9°, the author has tested the excitation switching sequence at from 6° to 11° difference. Tables 8 and 9 show the energy, torque, speed, flux linkage, current, voltage while changing excitation voltage and losses. It has been examined that the starting torque of the machine remains same and have no effect on changing the switching sequence whereas the average

torque is improved as the higher degree of difference in switching angle is given to switches however there is an increasing trend effect on speed as the angle difference is increased. Fig. 10, shows the harmonics and back emf graph while varying switching sequence and it can be finally concluded that the switching angle directly affecting the harmonics and back emf. The maximum harmonics up to 29.8% produced at 50% slot filling factor in between the coil 1 and 2 whereas the maximum back emf is produced up to 84 V in between the same coil 1 and 2 at 45% slot filling factor as shown in Figs. 11a and b.

4 Conclusion

The design of a 12/8 SRM has been presented in the paper. The design looks into the parameters such as the switching pattern, slot filling factor and winding excitation voltage. The simulation results confirmed the good characteristics of SRM particularly back emf and harmonic contents, as high efficiency is expected to be
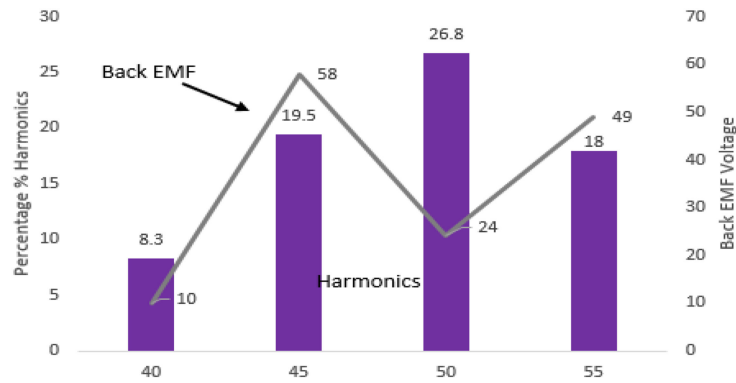
Fig. 8 *Harmonics and back emf with the filling factor and the number of turns*

Table 6 Energy, torque, speed and flux linkage while changing excitation voltage

| Voltage | Energy | | Torque in, N m | | Speed in, degree/sec | | Flux linkage |
	Inst	Co-energy	Start	Avg	Max	Avg	Max
200	19.7	47	275	41	16,200	9739	0.13
150	8.3	14	198	22	15,200	8608	0.07
100	3.8	5.8	145	9.1	5800	4189	0.07
50	1.9	2.2	55	4.5	3300	2511	0.06

Table 7 Current, voltage and losses while changing excitation voltage

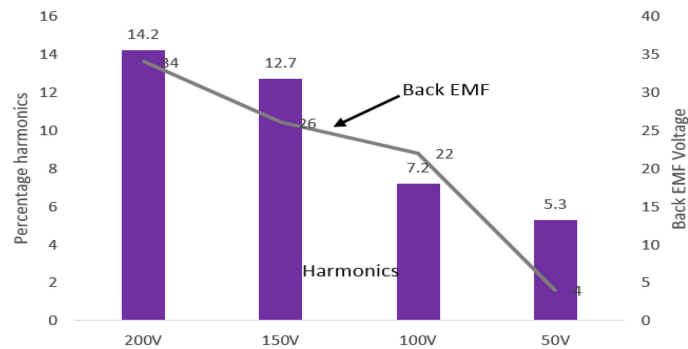| Voltage	Current	Voltage	Ohmic loss	Iron loss
200	13	29	74	36.7
150	6	8.9	15	19.9
100	4.7	10	4.2	13.7
50	3.1	3.2	1.1	6.6

Fig. 9 *Harmoinc and back emf graph while varying excitation voltage*

Table 8 Energy, torque, speed and flux linkage while changing switching sequence

| Difference | Energy | | Torque in, N m | | Speed in, degree/sec | | Flux linkage |
	Inst	Co-energy	Start	Avg	Max	Avg	Max
6	7.3	17.7	275	12	7400	5731	2.09
7	9.3	20.4	275	19	9700	6582	6.1
8	16.5	41.7	275	31	16,100	7376	23.9
9	19.7	47.7	275	41	16,200	9739	29
10	10.1	21.9	275	22	15,800	7081	30.8
11	13.8	29.6	275	30	15,400	7633	21.1

Table 9 Current, voltage and losses while changing switching sequence

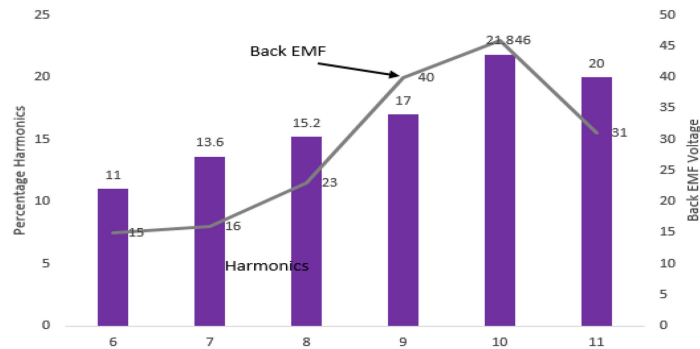| Difference	Current	Voltage	Ohmic loss	Iron loss
6	7.7	2.09	25.5	19.9
7	9	6.1	28.1	21.6
8	13.6	23.9	63.9	31.3
9	13	29	74.9	36.7
10	10.8	30.8	28.9	25.3
11	14.2	21.1	35.6	34.4

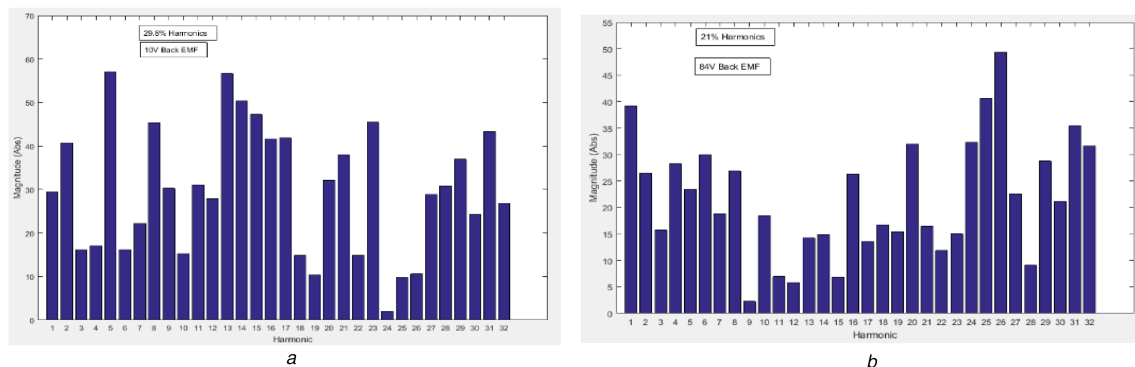**Fig. 10** *Harmoinc and back emf graph while varying excitation switching sequence*

Fig. 11 *Harmonic results*
(a) Maximum harmonics, *(b)* Maximum back emf produced in 12/8 SRM

achieved through this optimised design and has the great potential to be used in electric vehicles.

5 References

[1] Bose, B.K.: 'Global warming: energy, environmental pollution, and the impact of power electronics', *IEEE Ind. Electron. Mag.*, 2010, **4**, pp. 6–17
[2] Ekwurzel, B., Boneham, J., Dalton, M.*, et al.*: 'The rise in global atmospheric CO_2, surface temperature, and sea level from emissions traced to major carbon producers', *Clim. Change*, 2017, **144**, pp. 579–590
[3] Hutchins, M.G., Colby, J.D., Marland, G.*, et al.*: 'A comparison of five high-resolution spatially-explicit, fossil-fuel, carbon dioxide emission inventories for the United States', *Mitigation Adapt. Strateg. Glob.Change*, 2017, **22**, pp. 947–972
[4] Bukhari, S.A.A.S., Cao, W.P., Soomro, T.A.*, et al.*: 'Future of microgrids with distributed generation and electric vehicles', in Cao, W.P., Yang, J. (Eds.), '*Development and integration of microgrids*' (InTech, ed Rijeka, 2017), p. Ch. 03
[5] Güneralp, B., Zhou, Y., Ürge-Vorsatz, D.*, et al.*: 'Global scenarios of urban density and its impacts on building energy use through 2050'. Proc. of the National Academy of Sciences, 2017, p. 201606035
[6] Solano Rodriguez, B., Drummond, P., Ekins, P.: 'Decarbonizing the EU energy system by 2050: an important role for BECCS', *Climate Policy*, 2017, **17**, pp. 8945–8950
[7] Situ, L.: 'Electric vehicle development: the past, present & future'. 3rd Int. Conf. on Power Electronics Systems and Applications, 2009. PESA 2009, 2009, pp. 1–3
[8] Abid Ali Shah Bukhari, S., Cao, W., Samo, K.A.*, et al.*: 'Electrical motor drive technologies for green electric vehicle: a review', *Eng. Sci. Technol. Int. Res. J.*, 2017, **1**, pp. 1–10
[9] Widmer, J.D., Martin, R., Kimiabeigi, M.: 'Electric vehicle traction motors without rare earth magnets', *Sustain. Mater. Technol.*, 2015, **3**, pp. 7–13
[10] Bouzidi, I., Masmoudi, A., Bianchi, N.: 'Design and feature investigation of an IPM motor dedicated to propulsion applications', *COMPEL-The Int. J. Comput. Mathematics Electr. Electron. Eng.*, 2012, **32**, pp. 126–141
[11] Hori, Y.: 'Looking at cars 100 years in the future'. 2013 IEEE Int. Conf. on Mechatronics (ICM), 2013, pp. 31–35
[12] Anon: 'Rare-earth mining in China comes at a heavy cost for local villages' (ed: Guardian, 2012)
[13] Parry, S., Douglas, E.: 'In China, the true cost of Britain's clean, green wind power experiment: pollution on a disastrous scale'. Mail Online, 26, 2011

[14] Bogusz, P., Korkosz, M., Prokop, J.: 'Current harmonics analysis as a method of electrical faults diagnostic in switched reluctance motors'. IEEE Int. Symp. on Diagnostics for Electric Machines, Power Electronics and Drives, 2007. SDEMPED 2007, 2007, pp. 426–431
[15] Zhu, Z., Lee, B., Huang, L.*, et al.*: 'Contribution of current harmonics to average torque and torque ripple in switched reluctance machines', *IEEE Trans. Magn.*, 2017, **53**, pp. 1–9
[16] Xu, Z., Kim, M.-J., Lee, D.-H.*, et al.*: 'Characteristics analysis and comparison of conventional and segmental rotor type 12/8 switched reluctance motors'. 2016 IEEE Industry Applications Society Annual Meeting, 2016, pp. 1–7
[17] Elmutalab, M.A., Elrayyah, A., Husain, T.*, et al.*: 'Extending the speed range of a switched reluctance motor using a fast demagnetizing technique'. 2016 IEEE Energy Conversion Congress and Exposition (ECCE), 2016, pp. 1–7
[18] Takiguchi, M., Sugimoto, H., Kurihara, N.*, et al.*: 'Acoustic noise and vibration reduction of SRM by elimination of third harmonic component in sum of radial forces', *IEEE Trans. Energy Convers.*, 2015, **30**, pp. 883–891
[19] Aravind, C., Norhisam, M., Aris, I.*, et al.*: 'Double-rotor switched reluctance machine (DRSRM): fundamentals and magnetic circuit analysis'. 2011 IEEE Student Conf. on Research and Development (SCOReD), 2011, pp. 294–299
[20] Yang, Y., Schofield, N., Emadi, A.: 'Double-rotor switched reluctance machine (DRSRM)', *IEEE Trans. Energy Convers.*, 2015, **30**, pp. 671–680
[21] Schenk, M., Hofmann, A., Kambadur, S.K.*, et al.*: 'Harmonic superposition of conductor losses in switched reluctance machines'. 2015 17th European Conf. on Power Electronics and Applications (EPE'15 ECCE-Europe), 2015, pp. 1–10
[22] Zhu, Y.-f., Ge, Q.-x., Chen, H.*, et al.*: 'Study of switched reluctance motor drive system fed by voltage PWM rectifier'. 2010 Int. Conf. on Electrical Machines and Systems (ICEMS), 2010, pp. 859–862
[23] He, C., Hao, C., Qianlong, W.*, et al.*: 'Design and control of switched reluctance motor drive for electric vehicles'. 2016 14th Int. Conf. on Control, Automation, Robotics and Vision (ICARCV), 2016, pp. 1–6
[24] Argiolas, O., Nazeraj, E., Hegazy, O.*, et al.*: 'Design optimization of a 12/8 switched reluctance motor for electric and hybrid vehicles'. 2017 Twelfth Int. Conf. on Ecological Vehicles and Renewable Energies (EVER), 2017, pp. 1–10
[25] Yu, Q., Wang, X., Cheng, Y.: 'Determination of air-gap flux density characteristics of switched reluctance machines with conductor layout and slotting effect', *IEEE Trans. Magn.*, 2016, **52**, pp. 1–7